Journal of Magnetism and Magnetic Materials 330 (2013) 16–20

Contents lists available at SciVerse ScienceDirect

Journal of Magnetism and Magnetic Materials

journal homepage: www.elsevier.com/locate/jmmm

Micromagnetic simulation of critical current density of spin transfer torque switching in a full-Heusler $Co_2FeAl_{0.5}Si_{0.5}$ alloy spin valve nanopillar

H.B. Huang [a,c], X.Q. Ma [a,*], Z.H. Liu [a], F.Y. Meng [a], S.Q. Shi [b], L.Q. Chen [c]

[a] Department of Physics, University of Science and Technology Beijing, Beijing 100083, China
[b] Department of Mechanical Engineering, The Hong Kong Polytechnic University, Hung Hom, Kowloon, Hong Kong
[c] Department of Materials Science and Engineering, The Pennsylvania State University, University Park, PA 16802, USA

ARTICLE INFO

Article history:
Received 1 May 2012
Received in revised form
6 September 2012
Available online 26 September 2012

Keywords:
Micromagnetic simulation
Critical current density
Spin transfer torque switching
Heusler alloy
Spin valve nanopillar

ABSTRACT

We investigated the critical current density of spin transfer torque switching in a full-Heusler $Co_2FeAl_{0.5}Si_{0.5}$ alloy spin-valve nanopillar through micromagnetic simulations. The simulations explain the experimental results on the resistance versus external magnetic field and yield good agreement with the measured switching behavior. It is shown that different magnitudes of current densities and directions of external magnetic fields give rise to a shift of resistance hysteretic loop and a variable range of switching. We demonstrated that three critical current densities have different slopes with Gilbert damping constant α and spin polarization constant η, indicating that α and η have different contributions to the critical current densities. Furthermore, we found that the area of resistance–current hysteretic loop decreases as the nanopillar size decreases. The domain structures indicated that the magnetization reversals have different switching processes between small and large sizes of pillars.

1. Introduction

In recent years, spin transfer torque (STT) switching, proposed by Slonczewski [1] and Berger [2] in 1996, has attracted considerable attention due to its application in high density magnetic random access memory (MRAM). STT devices offer superior performances such as large storage density, high switching speed, low energy consumption, and avoidance of cross writing. Spin polarized electrons carry spin angular momenta from the fixed layer to the free layer. It causes free layer switching when the current density exceeds a critical current density J_c. However, the critical current density required to induce the STT-based magnetization dynamics in the spin-valves is as high as 10^6–10^8 A/cm^2, and it is challenging to reduce J_c to achieve the compatibility with highly scaled complementary metal-oxide-semiconductor technology while maintaining the thermal stability.

The critical current density for spin transfer torque switching can be estimated by taking into account both spin pumping and the finite penetration depth of the transverse spin current [3–5]. In the macrospin approximation model, J_c at zero temperature can be described as

$$J_c = \frac{2e\alpha M_s t_F (H + H_k + 2\pi M_s)}{\hbar\eta} \quad (1)$$

where α is the Gilbert damping constant, η is the spin polarization constant, M_s is the saturation magnetization, t_F is the thickness of the free layer, H is the external magnetic field, H_k is the magnetocrystalline anisotropy field, e is the elementary charge of an electron, and $\hbar$ is the reduced Planck constant. Many attempts have been made to reduce J_c, including using CoFeB as the free layer to reduce M_S; [6] with a double spin-filter structure, [7] an antiferromagnetic pinning structure, [8] or inserting a Ru spin scattering layer [9] to increase spin scattering, or using a composite free layer consisting of two ferromagnetic layers with various coupling types [10–13].

According to Eq. (1), Heusler alloys with lower M_s, smaller α and higher spin polarization factor η are excellent candidates for reducing J_c compared to CoFe, Fe, Co and Py. Experimental measurements of Aoshima et al. [14] showed that J_c of Co_2MnGe, Co_2FeSi, and $Co_{75}Fe_{25}$ spin-valves were 1.6×10^7, 2.7×10^7, and 5.1×10^7 J/cm^2, respectively. A large magnetoresistance ratio of 6.9% at room temperature (RT) for $Co_2FeAl_{0.5}Si_{0.5}$ (CFAS)/Ag/CFAS spin-valves was found.[15] Sukegawa et al.[16] first demonstrated efficient spin transfer switching in $Co_2FeAl_{0.5}Si_{0.5}$-based spin valve, and showed that the resistance–current curves exhibited a two-step switching process, originating from the interplay between the magnetocrystalline anisotropy of CFAS layers and STT. For both experiments and simulations of $Co_2FeAl_{0.5}Si_{0.5}$ spin valves under an appropriate negative current, there exists an intermediate (I) state with the direction of the magnetization perpendicular to their original antiparallel (AP) and final parallel (P) spin configurations, [16,17] i.e., the magnetization reversal from the initial AP state to

* Corresponding author. Tel.: +86 10 62334074; fax: +86 10 62327283.
E-mail address: xqma@sas.ustb.edu.cn (X.Q. Ma).

0304-8853/$ - see front matter © 2012 Elsevier B.V. All rights reserved.
http://dx.doi.org/10.1016/j.jmmm.2012.09.031

the I state and then to the P state as the current decreases, forming a two-step switching in the negative part of the hysteretic loop. For a positive current, there is only one-step switching, i.e., the magnetization reversal from P to AP directly. However, there have been no discussions on what kind of conditions will affect the magnitude of the critical current density in the Heusler-based spin valve, such as the external magnetic field, size of nanopillar, spin polarization constant and Gilbert damping constant.

In this paper, we investigated the critical current density of spin transfer torque switching in a full-Heusler $Co_2FeAl_{0.5}Si_{0.5}$ alloy spin-valve nanopillar through micromagnetic simulations. In addition to the observation of the two-step switching behavior under an external magnetic field, we demonstrated the shifts in the resistance versus current hysteretic loop and the variable range of I state under the external magnetic fields. Furthermore, our investigation also shows that the critical current density increases with Gilbert damping constant α and decreases with spin polarization constant η, which can be used to evaluate different strategies for reducing J_c in experiments. We also present the R–J hysteretic loops and the corresponding domain evolution as a function of the nanopillar size with roughly the same aspect ratio, indicating different switching mechanisms for different sizes.

2. Model description

A spin valve device was investigated with the geometry similar to the structure of spin valve in Ref. 16[CFAS (20 nm)/Ag (4 nm)/CFAS (2.5 nm)]. As shown in Fig. 1, we employed a Cartesian coordinate system where the x-axis is the long axis of the ellipse along the CFAS [110] direction (easy axis) and the y-axis is along the short axis ([$\bar{1}$10]). The two CFAS layers are separated by a thin Ag layer, and the bottom CFAS layer is the free layer whose magnetization dynamics is triggered by a spin-polarized current. The top CFAS layer is the pinned layer with its magnetization vector P fixed in the direction along the positive x axis. The initial magnetization vector M of the layer is along the negative or positive x axis. The middle Ag layer is a space layer whose function is to avoid the exchange coupling between the two CFAS layers. The thickness of the spacer layer (4 nm) is much smaller than the spin diffusion length to conserve the spin momentum. The positive current is generally defined as electrons flowing from the free layer to the pinned layer.

The magnetization dynamics is described by using a generalized Landau–Lifshitz–Gilbert–Slonczewski (LLGS) equation, [1] which can be written as

$$\frac{dM}{dt} = -\gamma' M \times H_{eff} - \frac{\alpha\gamma'}{M_s} M \times (M \times H_{eff}) - \frac{2\mu_B J}{(1+\alpha^2)edM_s^3} g(M,P) M \times (M \times P) + \frac{2\mu_B \alpha J}{(1+\alpha^2)edM_s^2} g(M,P)(M \times P) \quad (2)$$

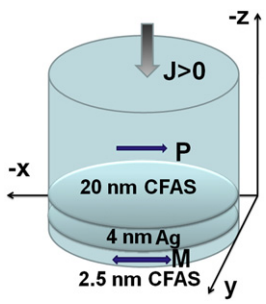

Fig. 1. Model geometry definition of CFAS (20 nm)/Ag (4 nm)/CFAS (2.5 nm) spin valve nanopillar in Cartesian coordinates.

where M is the magnetization of the free layer, P is the magnetization of the pinned layer, H_{eff} is the effective field, $\gamma' = \gamma/(1+\alpha^2)$, γ is the electron gyromagnetic ratio, and α is the dimensionless damping parameter. The effective field includes the anisotropy field, the demagnetization field, the external field and the exchange field, namely $H_{eff} = H_k + H_d + H_{ext} + H_{ex}$.

The last two terms on the right side of Eq. (2) describe STT that tends to drag the magnetization away from its initial state to its final state. The scalar function is given by [1]

$$g(M,P) = [-4 + (1+\eta)^3(3 + MP/M_s^2)/4\eta^{3/2}]^{-1} \quad (3)$$

where the angle between M and P is θ. $M \cdot P/M_s^2 = \cos\theta$.

H_{STT} is the corresponding effective field given by

$$H_{STT} = 2\mu_B J g(M,P) MP/(\gamma edM_s^3) \quad (4)$$

where μ_B, J, d, i, M_s, are the Bohr magneton, current density, thickness of the free layer, electron charge, and saturation magnetization, respectively.

We adopted the following magnetic parameters [16], saturation magnetization $M_s = 9.0 \times 10^5$ A/m, exchange constant $A = 2.0 \times 10^{-11}$ J/m, and magnetocrystalline anisotropy constant $K_1 = -1.0 \times 10^4$ J/m^3. Other parameters are Gilbert damping parameter $\alpha = 0.01$, and spin polarization factor $\eta = 0.76$. The dynamics of magnetization was investigated by numerically solving the time-dependent LLGS equation using the Gauss–Seidel projection method [18,19] with a constant time step $\Delta t = 23.8993$ fs for getting the results exactly. The samples were discretized in computational cells of $2.5 \times 2.5 \times 2.5$ nm^3 [20–22].

3. Results and discussion

We investigated the critical current density of spin transfer torque switching in a full-Heusler $Co_2FeAl_{0.5}Si_{0.5}$ alloy spin-valve nanopillar with a device area of 250×190 nm^2. As shown in Fig. 2, the relative resistance versus external magnetic field (R–H) hysteretic loops were simulated with different positive current densities, and the external magnetic field is along the $+x$ or $-x$ axis. A two-step magnetization switching behavior, as observed experimentally [16] was obtained at a constant current density of 2.5×10^5 A/cm^2, and the curve yields good agreement with the experimental results. In the R–H curves, three states are evident: the parallel (P), antiparallel (AP), and intermediate (I: perpendicular to P) states. For one-step switching, the magnetization flips from P to AP are above the critical magnetic field. While for the two-step switching, the magnetization flip from AP to I first at a smaller magnetic field. Then, it switches from I to P at a larger field. We attributed this two-step switching to the fourfold in-plane

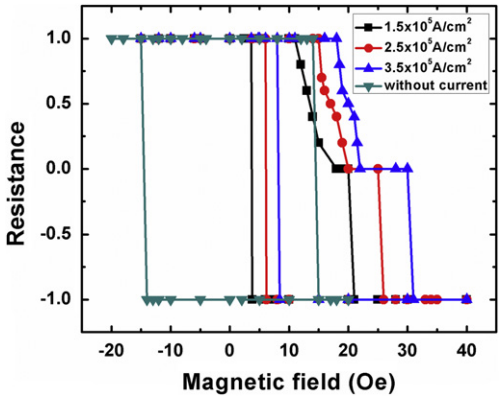

Fig. 2. Resistance versus external magnetic field (R–H) hysteretic loop at different current densities.

magnetocrystalline anisotropy of CFAS layers [17]. The hysteresis offset field (H_{offset}) acquired from the R–H curves is 16 Oe at a constant current density of 2.5×10^5 A/cm^2, which is in agreement with the experiments [16]. Furthermore, we changed the current value to determine the character of current in the magnetization switching. As shown in Fig. 2, we found that the R–H loop shifts to right or left as the current density increases to 3.5×10^5 A/cm^2 or decreases to 1.5×10^5 A/cm^2, respectively. The positive spin polarization current drags the free layer magnetization to the antiparallel direction, and hence the magnetization of P is unstable and easy to switch from P to AP as current density increases. The critical field of switching from P to AP decreases with the current and increases with the reverse current from AP to P. Therefore, we can conclude that the change in current density could lead to shift of the R–H hysteretic loops. We also simulated the R–H hysteretic loop without current. The offset field H_{offset} in this case is equal to 0. The two-step switching disappears when the current density decreases to zero, leading to a symmetric hysteresis loop, indicating that the spin polarization current is the primary reason for the unsymmetrical hysteresis loop as shown in our previous paper [17].

Fig. 3 shows the relative resistance R as a function of current density (R–J) at various directions of external magnetic fields in the CFAS/Ag/CFAS nanopillar. All four R–J hysteretic loops exhibit two-step switching behavior. Under the magnetic field of 12 Oe along the $+x$ axis, J_{c1}^- for AP to I does not change while J_{c2}^- for I to P increases from -9.0×10^6 A/cm^2 to -8.0×10^6 A/cm^2 and J_c^+ for P to AP increases from 2.5×10^7 A/cm^2 to 3.5×10^7 A/cm^2. This can be explained by the fact that the external field along the $+x$ axis has a slight effect on the magnetization switching from AP to I, and it favors the switching from I to P, dragging the magnetization to the $+x$ axis. The Slonczewski's model takes into account the interface spin-flip scattering effect. STT versus θ is described by Eq. (5), and STT reaches its maximum at an angle θ larger than 90°, leading to a larger magnitude of STT at I (90°) than that at AP (180°) [17]. It is easy to reverse from I to P than AP to I under an external field along $+x$ axis. However, the external field along the x-axis impedes the switching from P to AP under a positive current. Therefore, the hysteretic loop shifts to the right under the $+x$ axis external magnetic field and vice versa. This agrees with the experiment [16] that the range of half-switching is reduced for the applied external field along the $+x$ axis.

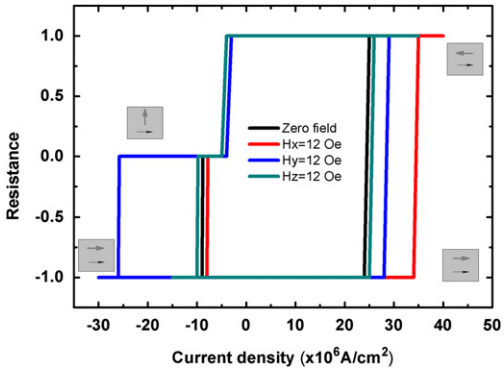

Fig. 3. External magnetic field dependence of resistance versus current density curves of CFAS/Ag/CFAS nanopillar.

There is a large decrease of J_{c2}^- from I to AP when the external magnetic field of 12 Oe is along the $+y$ axis. It causes the magnetization to stay in the $+y$ axis (I state), hindering the magnetization switching from I to P. The field is also promoting the switching from AP to I, while impeding the switching from P to AP. Therefore, the loop under the $+y$ axis external field shifts to the left for the negative current density and to the right for the positive current density. The range of half-switching current increases as the magnitude of external field along the $+y$ axis increases. Additionally, the $+z$ axis external field always impedes the magnetization switching to x axis in both current directions since the magnetization does not flip to the z axis. So the area of the loop under the $+z$ axis external field is larger than that under the zero field, and it requires overcoming higher barrier to switch the magnetization in both positive and negative current densities.

In order to understand the variation of the critical current density J_c with Gilbert damping constant α and spin polarization constant η in CFAS/Ag/CFAS nanopillar, we performed a set of numerical simulations. We obtained three curves with different slopes, showing different effects of α and η on J_c. The "Gilbert damping" of the second term of Eq. (2) takes into account of energy dissipation as a result of coupling to lattice vibrations[21] and spin-flip scattering [23,24] although there is an active debate whether this form of the damping is correct [25–27]. The large α value may result from the inhomogeneity due to porosity [28–30] since the pores at a grain boundary cause the non-uniformity in the internal magnetizing field or non-uniform demagnetizing field due to the internal defect. In addition, high spin polarization current contributes to the large magnetoresistance ratios in spin valves using half-metallic full-Heusler alloys [31–33].

Fig. 4 shows the distribution of the values of J_c as a function of Gilbert damping constant α and reciprocal of spin polarization constant $1/\eta$. Wang et al. investigated the relationships of J_c vs α and η, and their obtained theoretical limit of critical current density is far below the present lowest critical current density [34]. There are three

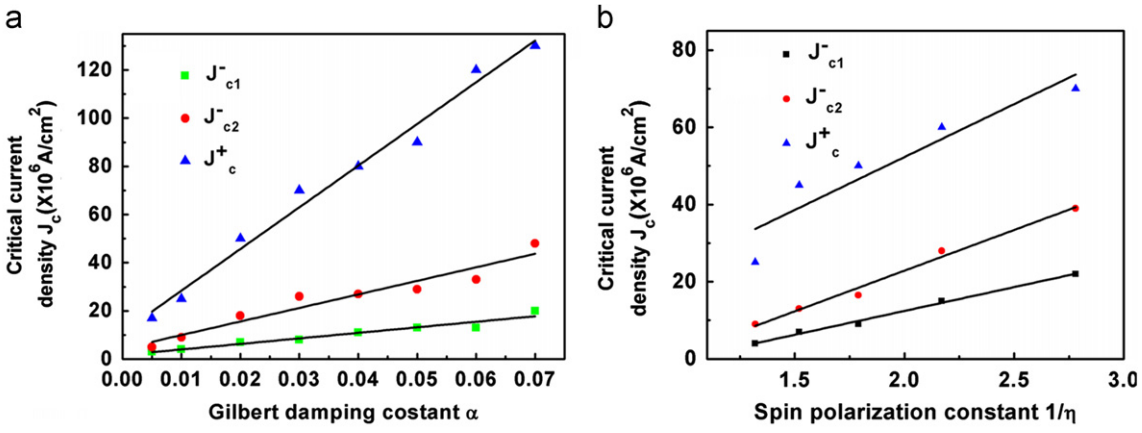

Fig. 4. (a) Critical current density versus Gilbert damping constant α for $\eta=0.76$ and (b) critical current density versus spin polarization constant η for $\alpha=0.01$ in the full-Heusler $Co_2FeAl_{0.5}Si_{0.5}$ alloy spin valve nanopillar.

critical current density values in the spin valve nanopillar CFAS/Ag/CFAS because of the two-step switching. We simulated the three curves of critical current densities and found a linear increase in critical current density with α and $1/\eta$, similar to the macrospin approximation model and Wang's theoretical prediction. However the slopes of three curves are different, indicating that α and η have different contributions to J_c. Eq. (1) is derived for the case of uniaxial in-plane anisotropy when the applied magnetic field is parallel to the anisotropy axis. However, CFAS of Hesuler alloy possesses four-fold in-plane magnetic anisotropy. Therefore, the slopes are different as a function of the Gilbert damping constant and spin polarized constant. This implies that we should multiply different constants while using Eq. (1) of the macrospin model to get the critical current density of spin transfer switching in Heuslor alloy spin valve. In Fig. 4(a), J_c is plotted versus Gilbert damping constant α using an experimental value of $\eta=0.76$ for the full-Heusler alloy CFAS.[16] For $\alpha=0.005$, J_{c2}^{-} from I to P is -5.0×10^6 A/cm^2, and J_c^{+} from P to AP is 1.7×10^7 A/cm^2. As α increases, all the three critical current densities increase.

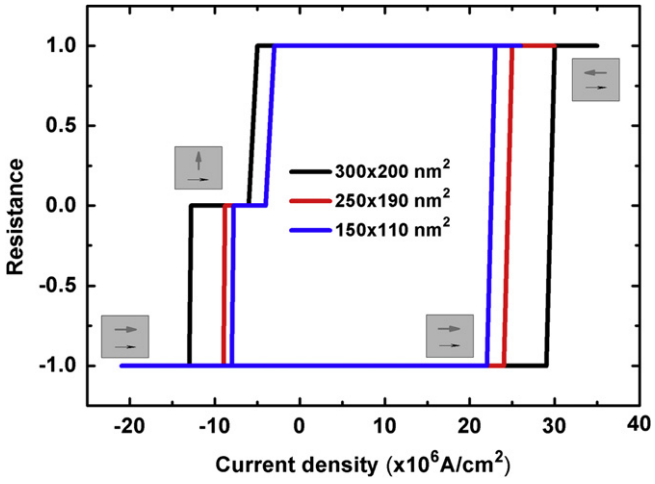

Fig. 5. Size dependent resistance as a function of current density of CFAS/Ag/CFAS nanopillar.

For example, for $\alpha=0.04$, J_c^{+}, J_{c1}^{-} and J_{c2}^{-} increase to 8.0×10^7 A/cm^2, -1.1×10^7 A/cm^2, and -2.7×10^7 A/cm^2, respectively. It is shown that increase in J_c^{+} with α is faster than J_{c1}^{-} and J_{c2}^{-}. This is also due to the fact that the relationship of STT versus θ (the angle between M and P) is not symmetric with respect to 90° in the Slonczewski's model[1], and thus the switching from AP to P is easier than that from P to AP [15]. Fig. 4 (b) describes the relationship between J_c and $1/\eta$ at $\alpha=0.01$. The three curves indicate that J_c^{+} increases faster with $1/\eta$ than J_{c1}^{-} and J_{c2}^{-}. These results may give guidance to the design of experiments.

Fig. 5 shows the R–J hysteretic loops as a function of device areas assuming approximately the same aspect ratios (1.3–1.5). The values of J_c in all cases are in good agreement with the experimental results [16]. The critical current density values from the simulations are $J_{c1}^{-}=-6.0\times10^6$ A/cm^2, $J_{c2}^{-}=-1.3\times10^7$ A/cm^2 and $J_c^{+}=3.0\times10^7$ A/cm^2 for the 300×200 nm^2 ellipse, and $J_{c1}^{-}=-4.0\times10^6$ A/cm^2, $J_{c2}^{-}=-8.0\times10^6$ A/cm^2 and $J_c^{+}=2.3\times10^7$ A/cm^2 for the 150×110 nm^2 ellipse. It is shown that the larger the device area, the larger the critical current densities are. STT has to overcome larger coercivity in a larger size of nanopillar to switch from the initial state to the final state. Therefore, the area of hysteretic loop also increases with the device area except for sizes below a critical dimension at which the magnetization structure is a single domain. Other groups [35,36] also reported that there is a rough linear increase in J_c with device area in other materials systems. Heindl et al. [35] found that the dependence of J_c on the device size is a result of a non-uniform and complex magnetization reversal process due to the excitation of non-uniform mode oscillations in devices with large areas. In our previous work, [17] we also showed that the switching is first excited at the boundaries of the structure via the nucleation process. They expand to the center of the structure and cause the formation of multi-domains, showing non-uniform magnetization reversal. We focus on the size-dependence of J_c due to different coercivity at the device with roughly the same aspect ratio. The magnetization reversals for all the three pillars are non-uniform switching process except for single-domain switching for pillar size smaller than the critical size for multidomain formation.

We now discuss the different switching mechanisms for large and small size nanopillars. Fig. 6 shows snapshots of the main steps of spin-transfer switching processes from AP to P at the

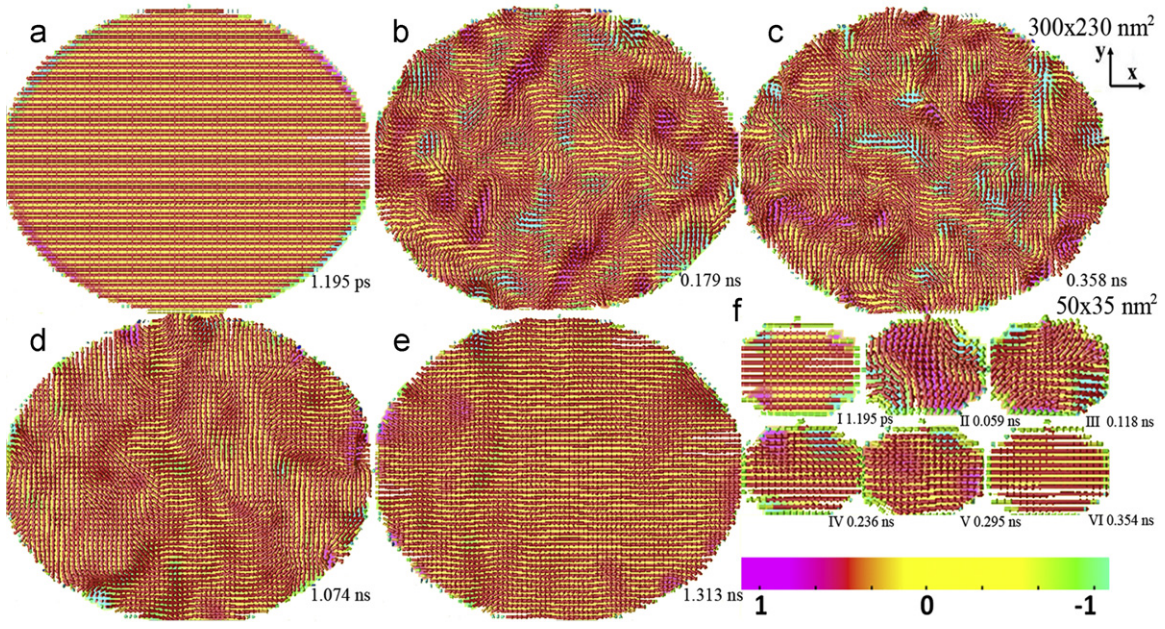

Fig. 6. Snapshots of magnetization distribution in the free layer. The colors represent the average magnetization component of $<mz>$ (red positive, cyan negative). (a)–(e) domain structures for the 300×230 nm^2 ellipse (f) domain structures for the 50×35 nm^2 ellipse.

current density of 1.3×10^7 A/cm^2 for a 300×250 nm^2 ellipse and at the current density of 4.8×10^7 A/cm^2 for a 50×35 nm^2 ellipse. The colors represent the average magnetization components of $<m_z>$. In Fig. 6(a), there is a single domain in the initial state and all the magnetizations are along the $-x$ axis. Then, this free layer will change to a multi-domain structure in Fig. 6(b) and (c) driven by the spin polarization current. Due to the fourfold in-plane magnetocrystalline anisotropy, both 90° and 180° domain walls are observed with more complex domain structures than normal metal nanopillars [21,35]. The magnetization at each point of the free layer experiences a torque exerted by STT. STT has no effect on the 180° domain (the magnetization along $+x$ or $-x$ axis) because H_{stt} is zero when the angle θ is 0° or 180°. The 90° domain (the magnetization along $+y$ or $-y$ axis) experiences a torque from the spin polarization current, and the area of 90° domain decreases and eventually disappears in Fig. 6(e). However, the switching process of single domain for a pillar smaller than the critical size for multidomain formation is very different. From Fig. 6(f), the single domain switching takes place from I (initial state along the $-x$ axis) to VI (final state along the $+x$ axis), and all the intermediate states have uniform magnetization direction.

4. Conclusions

We investigated the critical current density of spin transfer torque switching in a full-Heusler $Co_2FeAl_{0.5}Si_{0.5}$ (CFAS) alloy spin-valve nanopillar using micromagnetic simulations. We concluded that the four-fold in-plane magnetocrystalline anisotropy results in a two-step switching with the asymmetry in the switching loop caused by the spin polarization current. Furthermore, both the current density and the external magnetic field may lead to the shift of R–H or R–J hysteretic loops, which is consistent with the experimental observations. In addition, the range of half-switching varies with the magnetic field; it decreases with an external field along the $+x$ axis and increases with an exernal field along the $+y$ axis. We demonstrated that the critical current densities decrease with the Gilbert damping constant α and the reciprocal of spin polarization constant $1/\eta$, in agreement with the macrospin approximation model. Finally, the critical densities decease with the device area except for sizes below a critical dimension at which the magnetization structure is a single domain. The magnetization reversal of larger size of pillar shows the non-uniform switching process while the single domain switching shows uniform magnetization.

Acknowledgments

This work was sponsored by the National Science Foundation of China (11174030), by the US National Science Foundation under the Grant number DMR-1006541 (Chen) and in part by the China Scholarship Council. The computer simulations were carried out on the LION and Cyberstar clusters at the Pennsylvania State University.

References

[1] J.C. Slonczewski, Journal of Magnetism and Magnetic Materials 159 (1996) L1.
[2] L. Berger, Physical Review B 54 (1996) 9359.
[3] J.A. Katine, F.J. Albert, R.A. Buhrman, M.B. Myers, D.C. Ralph, Physical Review Letters 84 (2000) 3149.
[4] J.Z. Sun, Physical Review B 62 (2000) 570.
[5] T. Taniguchi, H. Imamura, Physical Review B 78 (2008) 224421.
[6] K. Yagami, A.A. Tulapurkar, A. Fukushima, Y. Suzuki, Applied Physics Letters 85 (2004) 5634.
[7] G.D. Fuchs, I.N. Krivorotov, P.M. Braganca, N.C. Emley, A.G.F. Garcia, D.C. Ralph, R.A. Buhrman, Applied Physics Letters 86 (2005) 152509.
[8] K.J. Lee, T.H.Y. Nguyen, K.H. Shin, Journal of Magnetism and Magnetic Materials 304 (2006) 102.
[9] Y. Jiang, S. Abe, T. Ochiai, T. Nozaki, A. Hirohata, N. Tezuka, K. Inomata, Physical Review Letters 92 (2004) 167204.
[10] H. Meng, J.P. Wang, Applied Physics Letters 89 (2006) 152509.
[11] Y. Zhang, Z. Zhang, Y. Liu, B. Ma, Q.Y. Jin, Applied Physics Letters 90 (2007) 112504.
[12] X. Li, Z.Z. Zhang, Q.Y. Jin, Y.W. Liu, Applied Physics Letters 92 (2008) 122502.
[13] C.T. Yen, W.C. Chen, D.Y. Wang, Y.J. Lee, C.T. Shen, S.Y. Yang, C.H. Tsai, C.C. Hung, K.H. Shen, M.J. Tsai, M.J. Kao, Applied Physics Letters 93 (2008) 092504.
[14] K. Aoshima, N. Funabashi, K. Machida, Y. Miyamoto, K. Kuga, N. Kawamura, Journal of Magnetism and Magnetic Materials 310 (2007) 2018.
[15] T. Furubayashi, K. Kodama, H. Sukegawa, Y.K. Takahashi, K. Inomata, K. Hono, Applied Physics Letters 93 (2008) 122507.
[16] H. Sukegawa, S. Kasai, T. Furubayashi, S. Mitani, K. Inomata, Applied Physics Letters 96 (2010) 042508.
[17] H.B. Huang, X.Q. Ma, Z.H. Liu, F.Y. Meng, S.Q. Shi, L.Q. Chen, Journal of Applied Physics 110 (2011) 033913.
[18] X.P. Wang, C.J. García-Cervera, E. Weinan, Journal of Computational Physics 171 (2001) 357.
[19] J.X. Zhang, L.Q. Chen, Acta Materialia 53 (2005) 2845.
[20] Z.H. Xiao, X.Q. Ma, P.P. Wu, J.X. Zhang, L.Q. Chen, S.Q. Shi, Journal of Applied Physics 102 (2007) 093907.
[21] X.Q. Ma, Z.H. Xiao, P.P. Wu, J.X. Zhang, L.Q. Chen, S.Q. Shi, Journal of Applied Physics 103 (2008) 07B111.
[22] H.B. Huang, X.Q. Ma, T. Yue, Z.H. Xiao, S.Q. Shi, L.Q. Chen, Science China Astronomy, Mechenical and Physics 54 (7) (2011) 1227–1234.
[23] H. Suhl, IEEE Transactions on Magnetics 34 (2002) 1834.
[24] V. Kambersky, Canadian Journal of Physics 48 (1970) 2906.
[25] V.L. Safonov, Journal of Applied Physics 91 (2002) 8653.
[26] A. Rebei, M. Simionato, G.J. Parker, Physical Review B 69 (2004) 134412.
[27] S.F. Zhang, S.S.-L. Zhang, Physical Review Letters 102 (2009) 086601.
[28] F. Rivadulla, et al., Journal of Magnetism and Magnetic Materials 470 (1999) 196–197.
[29] H. Song, J. Oh, J. Lee, S. Choi, Physics of the Solid State 189 (2002) 829.
[30] C.J. Brower, C.E. Patton, Journal of Applied Physics 53 (1982) 2104.
[31] Y. Sakuraba, M. Hattori, M. Oogane, Y. Ando, H. Kato, A. Sakuma, T. Miyazaki, H. Kubota, Applied Physics Letters 88 (2006) 192508.
[32] W.H. Wang, H. Sukegawa, R. Shan, K. Inomata, Applied Physics Letters 93 (2008) 122506.
[33] R. Shan, H. Sukegawa, W.H. Wang, M. Kodzuka, T. Furubayashi, T. Ohkubo, S. Mitani, K. Inomata, K. Hono, Physical Review Letters 102 (2009) 246601.
[34] X.R. Wang, Z.Z. Sun, Physical Review Letters 98 (2007) 077201.
[35] R. Heindl, S.E. Russek, T.J. Silva, W.H. Rippard, J.A. Katine, M.J. Carey, Applied Physics Letters 92 (2008) 262504.
[36] M. Carpentieri, G. Consolo, B. Azzerboni, L. Torres, E. Cardelli, IEEE Transactions on Magnetics 43 (2007) 1677.